

All-optical control of the time delay in a one-dimensional photonic bandgap formed by double-quantum-wells

M.A. Antón ^{*}, F. Carreño, Oscar G. Calderón, Sonia Melle

Escuela Universitaria de Óptica, Universidad Complutense de Madrid, Cl Arcos de Jalón s/n, 28037 Madrid, Spain

Received 31 July 2007; received in revised form 27 September 2007; accepted 4 October 2007

Abstract

In this work, we show the feasibility of all-optical control of time delay in a Bragg grating with an active defect that consists in an asymmetric double quantum-well $GaAs/Al_xGa_{1-x}As$. The double quantum-well is modeled as a A - V -type four level system. The refractive index of the defect can be modified by a control field due to the tunneling-induced quantum interference. It is shown that index changes as large as 0.4 can be obtained via cross-phase modulation. This allows for the development of a propagating mode at the selected wavelength. The existence of the mode permits the slow-down of light pulses, thus the system may act as a delay line with a group index as high as 100 operating at bandwidths of tens of GHz. We demonstrate that this defective photonic bandgap structure could enable ultrafast and ultrasensitive nonlinear all-optical switching at moderate powers of the control field.

© 2007 Elsevier B.V. All rights reserved.

Keywords: Coherent optical effects; Quantum well structures; Slow light; All-optical switch

1. Introduction

Recent dramatic experimental demonstration of slow and fast light has stimulated considerable interest in the dynamic control of the group velocity of light and in the development of tunable all-optical delays for applications such as optical buffers. Two methods are generally exploited to control optical delay: one of them is by using dispersive devices and the other rests in the modification of the group index of an optical medium [1–6]. The first approach is structural, where one aims for finding an optimal structure that will enhance the nonlinear response (through its geometrical properties). Some of the most promising systems that explore this approach are Fabry–Perot resonators, high Q cavities, and photonic crystals. The second approach makes use of nonlinear optics such as electromagnetically induced transparency (EIT) [1–3], coherent population oscillation (CPO) [5], Raman [7,8] and Brillouin amplification [9–11]. These nonlinear optical techniques have been extensively

studied in atomic systems, however the corresponding counterparts in solid state crystals, fibers, and semiconductors would be extremely attractive in order to obtain optical tunable delay lines, buffers and other practical applications. EIT in a solid has been carried out with a rare-earth doped matrix [12]. Experimental results show a slow-down factor of 10^7 using EIT in a gas cell at 350 K and in a Pr:doped solid at 5 K [13]. Some of the usual coherent effects which are present in dilute systems have been investigated theoretically and experimentally in semiconductors [14–16]. In particular, EIT was experimentally obtained using exciton and biexciton transitions in a quantum-well (QW) structure [17–20]. There are additional studies on laser without inversion (LWI), refractive index enhancement in semiconductor nano-structures for coherent mid-to far-infrared radiation generation [21], optical storage [22], and for sensitive infrared detectors [23]. Several schemes for achieving EIT or LWI have been proposed, and the observation of a strong absorption reduction in intersubband transitions have been recently reported. In particular, Fano-type interferences in quantum well structures have been experimentally observed [24]. In addition, extremely useful devices such as ultrafast

^{*} Corresponding author. Tel.: +34 913946855; fax: +34 913946885.
E-mail address: antonm@fis.ucm.es (M.A. Antón).

optical switches [25,26], and quantum switches [27] based on Fano-type interferences in double quantum wells have been reported. In these cases the coherence is established by resonant tunneling which enables one to change the coupling strength with a bias voltage. Devices which take advantage of intersubband transitions in quantum wells have inherent advantages, such as slow-light effects at bandwidths greater than GHz, large electric dipole moments due to the small effective electron mass, and a great flexibility in the device design by a proper selection of the materials and their sizes. However, the fast decoherence of optical excitations in semiconductors imposes a severe limitation on the achievable group velocity reduction. Advances in atom-like semiconductor nanostructures such as quantum dots make possible the achievement of a large slow-down factor [28].

On the other hand, recent research efforts have been focused on replacing relatively bulky fiber-optic delay-line systems with compact integrated devices. Approaches have included the use of all-pass filters [29–31], coupled resonator optical waveguides [32–38] and Bragg gratings [39]. Photonic bandgap (PBG) materials represent a new type of optical medium, where the refractive index periodicity introduces optical bandgaps – energy bands with no available photon states – at frequencies where the optical wave vector is related to the grating wave vector. This leads to a high reflectance over a range of wavelengths which is proportional to the index contrast of the structure. In this sense, it is possible to engineer devices that enhance the interaction strength between the electromagnetic field and the medium. These devices are ultimately limited by the resonator quality factor Q . Moreover, tuning the time-delay requires precise spatial control over the thermal, optical, or electric control fields. Previous works in ideal 1D structures suggested that near a photonic band edge, a large delay tunability can be achieved for a small change in refractive index [39,40]. Pulses incident near the transmission band-edge resonances experience a group delay that is proportional to the density of modes of the band-gap. The density of modes exhibits abrupt changes at the edge of the gap, thus the group velocity for the incident pulse will be very small and the delay achieved could be very large. However, some complications emerge when designing an hetero-structure that places a particular wavelength at the band-edge resonances. The difficulties arise from the fact that the wavelengths positions of the resonances not only depend on the refractive indices of the distributed Bragg reflector (DBR) but on the number of layers. This fact makes unstable the band-edge position. In order to make use of the PBG platform advantages, Sadhegi et al. [41,42] have proposed one-dimensional bright and dark optical lattices where Bragg scattering occurs via EIT in a n-doped semiconductor quantum-well, which may be assimilated to a three-level atom, embedded in a waveguide structure.

In this work, we examine a similar approach to obtain an integrated tunable time-delay device by combining a resonant Bragg structure and a slow-light material. An exam-

ple of such a device is a 1D PBG, schematically shown in Fig. 1. The cavity consists of two PBG reflectors with a defect layer sandwiched in between, and placed inside of a PBG waveguide. We consider a defect formed by an asymmetric double quantum well structure where Fano-type interferences take place and allow for cross-phase modulation when both the signal and the control field are present. While the quantum well considered in Ref. [41] may be assimilated to a three level system where the coupling field produces electromagnetic induced absorption (EIA) accompanied by index enhancement for the probe field and operates at $5.87\ \mu\text{m}$, in our case the QW may be modeled as a four-level system of the A - V -type where EIT-like phenomenon is obtained even in the absence of the coupling field. In fact, the role of the coupling field in our structure is replaced by the interaction between intermediate subbands through tunneling, i.e., transparency arises from the destructive interference between the two optical paths $|2\rangle \leftrightarrow |1\rangle$ and $|3\rangle \leftrightarrow |1\rangle$ (see Fig. 1b). One can then envision inducing strong cross-phase modulation between the control and probe fields in such a way that a small change in the Rabi frequency of the control field induces a measurable shift of the position of the optical resonance which is accompanied by a change in the refractive index while keeping constant the absorption level. The operating principles of the considered structure relies in the fact that the defect introduces a phase shift which depends on its length (L_D) and its refractive index (n_D). For proper values of L_D and n_D a propagation mode appears at the desired wavelength into the band-gap which will allow for the corresponding reduction on the group velocity of light pulses. In particular, we illustrate our results by using real experimental parameters corresponding to the case of $\text{GaAs-Al}_x\text{Ga}_{1-x}\text{As}$ whose relevant conduction band energy levels are shown in Fig. 1. Schmidt et al. have observed tunneling induced transparency in this quantum well [24]. This structure operates at $9.36\ \mu\text{m}$. Although this range of the electromagnetic spectrum is of interest for detection purposes [23], a better frequency range for the probe field in the range of $1.5\ \mu\text{m}$ used for communications should be desirable. This would require an adequate selection of the materials in order to design the QW while maintaining the dephasing rates at such

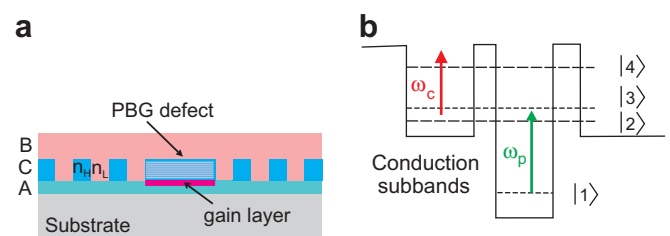


Fig. 1. (a) Schematic representation of a passive 1D photonic bandgap structure with an active defect site at its center. The corrugated QW structure is located between the upper and lower cladding layers. (b) Conduction subbands of the double quantum well in the bare basis.

levels that the coherence phenomena will be preserved. In this proof-of-principle study we have selected a QW where all the physical parameters required for simulations are disposable [26]. In addition, Fano-interferences have been proved experimentally to occur in this QW [24,26] and has been a subject of consideration [43]. All-optical bistability have been predicted to take place in this type of QW [44] and large cross-phase modulation could be achieved with vanishing both linear and two-photon absorption [45]. In this work we have tried to find convenient control parameters to make the advantages of semiconductor materials accessible for possible applications. In contrast to other works which obtain tunability by applying voltage [46–48] or temperature [49], here we propose a scheme that combines the resonant properties of the Bragg structure and the quantum coherence and interference properties in a double quantum well.

We also address the question of whether the proposed system may exhibit all-optical switching operation. This question has been previously considered in sophisticated systems with a high-finesse Fabry–Perot cavity containing ultracold resonant atoms [2,60]. Another exciting proposal based in a planar photonic crystal have been analyzed by Soljačić [61,62] in a hybrid photonic crystal microcavity where a single ultraslow light atom has been inserted at its center. They obtained all-optical switching at ultraslow energy levels via the cross-phase modulation produced in the N -type atomic system. In this work we show that a corrugated multiple quantum well embedded between Bragg reflectors may act as the semiconductor analog of the photonic crystal microcavity considered in [61]. In our case, tunneling-induced transparency can serve as the “second” arm in the V configuration of the EIT scheme. This approach differs from the usual N -type configuration in the fact that the tunneling scheme is not a time varying perturbation, such as the pump field which connects the two intermediate levels in the N -type atom, but a stationary ingredient of the double quantum-well. In view of this, we only use two coherent fields for obtaining the all-optical switching, whereas in the N -type atom based scheme three coherent fields are needed.

The paper is organized as follows: Section 2 establishes the model, i.e. the Hamiltonian of the system and the evolution equation of the atomic operators assuming the rotating wave approximation. Section 3 deals with the creation of a propagation mode in a corrugated structure which makes the system to act as a tunable filter and will allow for the slow-down of light. Section 4 summarizes the main conclusions.

2. Theoretical model. Absorptive and dispersive properties of a double QW

We consider the one-dimensional Bragg structure shown in Fig. 1a. It contains a substrate, lower and upper confinement layers (A and B), and a corrugated multi-QW structure (C). Here, the darker regions in the corrugated

multi-QW structure refer to the teeth of the gratings and the brighter regions to the trenches formed by etching the QW's and filling the trenches with another proper semiconductor material. The refractive index of the teeth/trenches is n_H/n_L . A defect is introduced at the center of the corrugated multi-QW structure. The defect is formed by several periods of a n -doped double QW structure which is shown schematically in Fig. 1b. It consists of two quantum wells that are separated by a narrow barrier. Below the defect a uniform gain layer is introduced in order to compensate for the losses. The system can be described by means of a four-level system where $|1\rangle$ and $|4\rangle$ are the ground state of the deep well and the first excited state of the shallow well, respectively. The states $|2\rangle$ and $|3\rangle$ are the result of mixing the ground state of the shallow well and the first excited state of the deep well when considered isolated each other.

The angular frequencies of the probe and control fields are ω_p and ω_c , respectively. Elementary processes to be taken into account comprise radiative excitation in both wells, electron tunneling between the wells, and relaxation of populations and polarizations. We assume that the carrier density in the double quantum well is low enough that an independent particle picture is valid [39,58,59]. In addition, we have taken the four subbands to have the same effective mass so the k -th dependence of the density matrix elements may be ignored. Thus we can model the coherent optical interactions using the atomic-like A - V -type four level system. This model is, of course, oversimplified. A more realistic model would include the influence of the interactions between carriers and the scattering of the carriers by phonons and disorders. Nevertheless, the present model can provide a good illustration of the optical processes of interest. The system is studied using the density-matrix formalism. The reduced density matrix in the interaction picture and in the rotating wave approximation read as

$$\frac{d\rho}{dt} = -\frac{i}{\hbar}[H_{\text{ext}}, \rho] + \frac{1}{2}L\rho, \quad (1)$$

where H_{ext} is the hamiltonian and L is the Liouvillian of the system, which are given by

$$H_{\text{ext}} = -\hbar[(\Delta_p + \Delta)\sigma_{22} + (\Delta_p - \Delta)\sigma_{33} + (\Delta_p + \Delta_c)\sigma_{44}] - \hbar(\Omega_p\sigma_{21} + q\Omega_p\sigma_{31} + \Omega_c\sigma_{42} + k\Omega_c\sigma_{43} + \text{H.c.}), \quad (2)$$

$$L = \gamma_4[2\sigma_{14}\rho\sigma_{41} - \sigma_{44}\rho - \rho\sigma_{44}] + \gamma_3[2\sigma_{13}\rho\sigma_{31} - \sigma_{33}\rho - \rho\sigma_{33}] + \gamma_2[2\sigma_{12}\rho\sigma_{21} - \sigma_{22}\rho - \rho\sigma_{22}] + \gamma_{32}[2\sigma_{13}\rho\sigma_{21} - \sigma_{23}\rho - \rho\sigma_{23}] + \gamma_{32}[2\sigma_{12}\rho\sigma_{31} - \sigma_{32}\rho - \rho\sigma_{32}], \quad (3)$$

where $\Delta_p = \omega_p - (\omega_{21} + \omega_{31})/2$ and $\Delta_c = \omega_c - (\omega_{42} + \omega_{43})/2$ denote the probe and control detunings, respectively, and $2\Delta = (\omega_{31} - \omega_{21})$ is the frequency splitting between levels $|2\rangle$ and $|3\rangle$. The corresponding Rabi frequencies are given by $\Omega_p = \mu_{21}E_p/2\hbar$, $\Omega_c = \mu_{42}E_c/2\hbar$. The parameters $q = \mu_{31}/\mu_{21}$

and $k = \mu_{43}/\mu_{42}$ represent the ratios between the dipole moments of the subband transitions.

The decay and dephasing rates $\gamma_i = \gamma_{il} + \gamma_{id}$ ($i = 2,3,4$) are included phenomenologically in the above equations. Here γ_{il} represents the population decay contribution and γ_{id} is the dephasing contribution originated from electron–electron scattering and electron–phonon scattering or even from quasi–elastic interface roughness. The crucial quantity giving rise to Fano interferences is $\gamma_{32} = \sqrt{\gamma_{2l}\gamma_{3l}}$ which denotes the mutual coupling between states $|2\rangle$ and $|3\rangle$ arising from the tunneling effect.

The possibility of decaying to the same continuum of states by resonant tunneling via an ultra-thin potential energy barrier, provides an effective coupling between the levels $|2\rangle$ and $|3\rangle$ [52]. It is well-known that the presence of an identical continuum for the decay of two energetically nearby states leads to asymmetric lineshapes due to Fano-type interferences [52]. These interferences have been experimentally observed in atomic systems, and in interband and intersubband transitions [53,54].

The Bloch equations for the density matrix elements including atomic spontaneous emission and dephasing are

$$\begin{aligned}
\frac{\partial \rho_{41}}{\partial t} &= -[\gamma_4 - i(\Delta_p + \Delta_c)]\rho_{41} - i\Omega_p \rho_{42} - iq\Omega_p \rho_{43} \\
&\quad + i\Omega_c \rho_{21} + ik\Omega_c \rho_{31}, \\
\frac{\partial \rho_{31}}{\partial t} &= -[\gamma_3 - i(\Delta_p - \Delta)]\rho_{31} - \gamma_{32}\rho_{21} + iq\Omega_p(\rho_{11} - \rho_{33}) \\
&\quad + ik\Omega_c^* \rho_{41} - i\Omega_p \rho_{32}, \\
\frac{\partial \rho_{21}}{\partial t} &= -[\gamma_2 - i(\Delta_p + \Delta)]\rho_{21} - \gamma_{32}\rho_{31} + i\Omega_p(\rho_{11} - \rho_{22}) \\
&\quad - iq\Omega_p \rho_{23} + i\Omega_c^* \rho_{41}, \\
\frac{\partial \rho_{43}}{\partial t} &= -[\gamma_3 + \gamma_4 - i(\Delta_c + \Delta)]\rho_{43} - \gamma_{32}\rho_{42} + ik\Omega_c(\rho_{33} - \rho_{44}) \\
&\quad - iq\Omega_p^* \rho_{41} + i\Omega_c \rho_{23}, \\
\frac{\partial \rho_{42}}{\partial t} &= -[\gamma_2 + \gamma_4 - i(\Delta_c - \Delta)]\rho_{42} - \gamma_{32}\rho_{43} + i\Omega_c(\rho_{22} - \rho_{44}) \\
&\quad + ik\Omega_c \rho_{32} - i\Omega_p^* \rho_{41}, \\
\frac{\partial \rho_{32}}{\partial t} &= -(\gamma_3 + \gamma_2 + i2\Delta)\rho_{32} - \gamma_{32}(\rho_{22} + \rho_{33}) + iq\Omega_p \rho_{12} \\
&\quad + ik\Omega_s^* \rho_{42} - i\Omega_p^* \rho_{31} - i\Omega_s \rho_{34}, \\
\frac{\partial \rho_{44}}{\partial t} &= -2\gamma_4 \rho_{44} + i\Omega_c \rho_{24} - i\Omega_c^* \rho_{42} + ik\Omega_c \rho_{34} - ik\Omega_c^* \rho_{43}, \\
\frac{\partial \rho_{33}}{\partial t} &= -2\gamma_3 \rho_{33} + \frac{\gamma_4}{2} \rho_{44} - \gamma_{32}(\rho_{32} + \rho_{23}) - ik\Omega_c \rho_{34} \\
&\quad + ik\Omega_c^* \rho_{43} + iq\Omega_p \rho_{13} - iq\Omega_p^* \rho_{31}, \\
\frac{\partial \rho_{22}}{\partial t} &= -2\gamma_2 \rho_{22} + \frac{\gamma_4}{2} \rho_{44} - \gamma_{32}(\rho_{32} + \rho_{23}) - i\Omega_c \rho_{24} \\
&\quad + i\Omega_c^* \rho_{42} + i\Omega_p \rho_{12} - i\Omega_p^* \rho_{21}.
\end{aligned} \tag{4}$$

The induced susceptibility in the intersubband transitions $|1\rangle \rightarrow |2\rangle$ and $|1\rangle \rightarrow |3\rangle$ is determined by

$$\chi(\omega_p, \Omega_c) = \chi_{\text{back}} + \frac{N|\mu_{21}|^2}{2\hbar\epsilon_0\Omega_p}(\rho_{21} + q\rho_{31}), \tag{5}$$

where N is the electron density in the conduction band of the double QW, and χ_{back} is the background susceptibility.

To evaluate the potential of this approach, we consider the quantum well structure depicted in Fig. 1b. This structure consists of a thick $Al_{0.4}Ga_{0.6}As$ barrier followed by a $Al_{0.16}Ga_{0.84}As$ shallow well (6.8 nm). This shallow well is separated from the $GaAs$ deep well (7.7 nm) on the right by a $Al_{0.4}Ga_{0.6}As$ potential barrier (3.0 nm). Finally, a thin (1.5 nm) $Al_{0.4}Ga_{0.6}As$ barrier separates the deep well from the last thick layer of $Al_{0.16}Ga_{0.84}As$ on the right. The dephasing rates are set to $\gamma_{2d} = 0.68$ meV, $\gamma_{3d} = 0.80$ meV, and $\gamma_{4d} = 0.50$ meV [26]. The population decay rates can be calculated by solving the Schrödinger equation for the double quantum well structure and it yields $\gamma_{2l} = 3.47$ meV, $\gamma_{3l} = 4.13$ meV, and $\gamma_{4l} = 0.80$ meV [26,50]. With these parameters, the Fano interference decay rate γ_{32} resulting for tunneling is $\gamma_{32} = \sqrt{\gamma_{2l}\gamma_{3l}} = 3.79$ meV. The energies of the levels of the double quantum-well are: $E_1 = 46.7$ meV, $E_2 = 174.8$ meV, $E_3 = 183.5$ meV, and $E_4 = 296.3$ meV (see Ref. [26]). The wavelength of the probe laser is around $9.36 \mu\text{m}$, which is accessible for some commercially available diode lasers. The dipole moments of these transitions are $\mu_{21} \simeq \mu_{31}$ ($q = 1$), and $\mu_{42} \simeq -\mu_{43}$ ($k = -1$).

Fig. 2a–b depicts the absorptive and dispersive response of the defect for the probe field for two values of the control field Ω_c versus the wavelength of the probe field λ_p . In the absence of the control field, $\Omega_c = 0$ (solid line) the atomic situation corresponds to a V -type atom where nearly EIT occurs via vacuum induced coherence or Fano interferences. Thus we recover the results obtained in Ref. [26]. In the vicinity of $\lambda_{p0} = 9.367 \mu\text{m}$ the medium becomes nearly transparent to the probe field. This transparency is accompanied by a steep variation of the refractive index (see solid line in Fig. 2b). Here, the role of the driving field in usual EIT experiments in gaseous media is played by the tunneling effect which couples the $|2\rangle \rightarrow |3\rangle$ transition. Wu et al. [26] demonstrated that when the control field is turned on and resonant ($\Delta_c = 0$), the system exhibits a strong absorption peak for the probe field. However, in this paper we will operate with a non-resonant control field since we are interested in maintaining a nearly transparent situation while changing the dispersion, thus we assume that the control field is detuned by about $\Delta_c = -2\gamma_2$. When Ω_c is set to a weak non-null value and far detuned from the $|2\rangle \rightarrow |4\rangle$ and $|3\rangle \rightarrow |4\rangle$ transitions, the absorption curve shifts and exhibits a minimum at $\lambda_{p1} = 9.428 \mu\text{m}$. This non-resonant field effectively changes the energy of the states $|2\rangle$ and $|3\rangle$ by an amount proportional to the Rabi frequency of the control field and induces an effective Stark shift of the resonant frequency which is smaller than the width of the transparency window. The medium will still remain nearly transparent for the probe field, but its refractive index experiences an appreciable enhancement (see Fig. 2b, dashed line) via cross-phase modulation. This behavior have some similarities to the giant nonlinearities that have been theoretically predicted in a N -type four-level atom [55,56], and recently observed in a four-level atomic

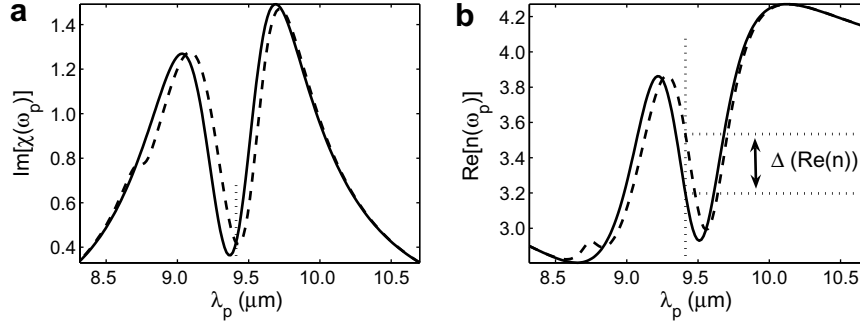


Fig. 2. (a) Absorption coefficient versus wavelength of the probe field λ_p . (b) Refractive index versus wavelength. Solid line corresponds to $\Omega_c = 0$ and dashed line to $\Omega_c = 0.5\gamma_2$.

system [57]. In summary, a small change in the Rabi frequency of the control field results in a large change of the refractive index. As we will see below, this change in the refractive index of the defect in the Bragg structure causes a phase shift in the field propagating through the Bragg structure allowing for the appearance of a propagating mode inside the bandgap.

Note that the two absorption curves have an intersection point between λ_{p0} and λ_{p1} . This point appears at $\lambda_{pd} = 9.4115 \mu\text{m}$ (see the vertical dotted line in Fig. 2a). Thus, a pulse with a carrier wavelength at λ_{pd} will experience a similar absorption when the control field Ω_c is turned on ($\Omega_c = 0.5\gamma_2$) and off ($\Omega_c = 0$), although the refractive indices will be different in both cases, due to the strong index enhancement achieved at λ_{pd} (see the double arrow in Fig. 2b) in the order of 0.4.

The existence of a non-null absorption at λ_{p0} and λ_{p1} arises from the dephasing contributions γ_{id} ($i = 2, 3, 4$) originated from electron-electron scattering and electron-phonon scattering. Even by letting $\gamma_{id} \rightarrow 0$, the absorption curve will show a non-null value due to the difference between γ_{2l} and γ_{3l} .

In order to make the results more transparent, we resort to obtain a simple analytical expression for the susceptibility by assuming a weak probe field. Thus, we can take $\rho_{11} \simeq 1$ in Eq. (4), and after some calculations we obtain the following expression for the first-order optical susceptibility experienced by the probe field, $\chi^{(1)}(\omega_p, \Omega_c)$, which reads as

$$\chi^{(1)}(\omega_p, \Omega_c) = i \frac{N|\mu_{21}|^2}{2\hbar\epsilon_0} \frac{|\Omega_c|^2(k-q)^2 + (q^2\Gamma_2 + \Gamma_3)\Gamma_4 - 2q\Gamma_4\gamma_{32}}{(\Gamma_2\Gamma_3 - \gamma_{32}^2)\Gamma_4 + |\Omega_c|^2(\Gamma_3 + k^2\Gamma_2 - 2k\gamma_{32})}, \quad (6)$$

where the Γ 's are given by

$$\begin{aligned} \Gamma_2 &= \gamma_2 - i(\Delta_p + \Delta), \\ \Gamma_3 &= \gamma_3 - i(\Delta_p - \Delta), \\ \Gamma_4 &= \gamma_4 - i(\Delta_p + \Delta_c). \end{aligned} \quad (7)$$

By assuming that $\Delta_c \gg \gamma_4$, Δ_p and $\gamma_2 \simeq \gamma_3$, which is adequate to the situation considered in the numerical calculations, Eq. (6) can be further approximated to get

$$\begin{aligned} \text{Re}(\chi^{(1)}(\omega_p, \Omega_c)) &\simeq \frac{N|\mu_{21}|^2}{\hbar\epsilon_0} \frac{(A_p - s_c)(\gamma_2^2 - \gamma_{32}^2 + \Delta^2)}{(\gamma_2^2 - \gamma_{32}^2 + \Delta^2)^2 + 4\gamma_2^2(A_p - s_c)^2} \\ &\simeq \frac{N|\mu_{21}|^2}{\hbar\epsilon_0} \frac{A_p - s_c}{\gamma_{\text{ef}}^2} \end{aligned} \quad (8)$$

$$\begin{aligned} \text{Im}(\chi^{(1)}(\omega_p)) &\simeq \frac{N|\mu_{21}|^2}{\hbar\epsilon_0} \frac{(\gamma_2 - \gamma_{32})(\gamma_2^2 - \gamma_{32}^2 + \Delta^2) + 2\gamma_2(A_p - s_c)^2}{(\gamma_2^2 - \gamma_{32}^2 + \Delta^2)^2 + 4\gamma_2^2(A_p - s_c)^2} \\ &\simeq \frac{N|\mu_{21}|^2}{\hbar\epsilon_0} \left[\frac{\gamma_2 - \gamma_{32}}{\gamma_{\text{ef}}^2} + 2\gamma_2 \left(\frac{A_p - s_c}{\gamma_{\text{ef}}^2} \right)^2 \right], \end{aligned} \quad (9)$$

where

$$s_c = \frac{\gamma_2 + \gamma_{32}}{\gamma_2\Delta_c} |\Omega_c|^2, \quad \text{and} \quad \gamma_{\text{ef}}^2 = \gamma_2^2 - \gamma_{32}^2 + \Delta^2. \quad (10)$$

A close look at Eqs. (8),(9) provides us an explanation of the different features obtained in the absorption and dispersion of the probe field. When the control field is turned off ($\Omega_c = 0$, then $s_c = 0$), a dip is obtained in the absorption spectrum at $\Delta_p = 0$ due to the presence of the factor $\gamma_2 - \gamma_{32}$. That is, the occurrence of Fano-type interferences are essential in this system. In the limit case that $\gamma_2 \rightarrow \gamma_{23}$, a perfect vacuum induced transparency is achieved. The effect of a non null nonresonant control field ($\Omega_c \neq 0$) becomes evident since it produces a Stark-shift of levels $|2\rangle$ and $|3\rangle$ and thereby shifts the spectrum by an amount given by s_c . This linear estimation agrees with the numerical findings depicted in Fig. 2. Furthermore, due to the stepness of the dispersion curve in the vicinity of the resonance, this Stark shift leads to a large phase shift, ϕ_p , along with small absorption of the probe field given by

$$\phi_p = \frac{2\pi N|\mu_{21}|^2 L_D}{\hbar\lambda_{pd}\epsilon_0} \frac{|\Omega_c|^2}{\Delta^2\Delta_c}. \quad (11)$$

We will exploit this giant Kerr cross-phase modulation to manipulate the optical properties of this material considered as a defect inside two DBR's.

3. All-optical generation of a propagation mode in a photonic bandgap

The quantum well structure itself induces a slow-down of light by EIT. However, when the quantum well structure

is incorporated at the center of a Bragg structure as a defect, the slow-down factor will be increased due to the resonant phenomenon occurring by interference between the forward and backward waves in the Bragg structure. Specifically, it is well-known that if the defect causes a π phase shift for the Bragg wavelength, the photonic bandgap can be changed and a propagation mode appears. This fact will serve us to obtain (i) a tunable transmission filter, (ii) all-optical control of time delay of light pulses propagating through the structure, and (iii) all-optical switching. In our case, the index of refraction of the defect can be changed dynamically by the control field as we have shown in the previous section. In order to confirm these effects we consider the optical response of a corrugated multi-QW structure which is embedded between two optical confinement layers, forming a periodic structure with a Bragg wavelength near to the intersubband transition $|1\rangle \rightarrow |3\rangle$ as depicted in Fig. 1b.

We are interested in the linear response of the layered structure, thus we can adopt a transfer matrix method [51]. The electric field amplitudes of waves propagating in forward and backward directions in the i -th layer are E_i^+ and E_i^- , respectively. After imposing the continuity of tangential components of E and H fields at the interface separating the i -th and $(i + 1)$ -th layers, the following matrix equation results:

$$\begin{pmatrix} E_i^+ \\ E_i^- \end{pmatrix} = T_i \begin{pmatrix} E_{i+1}^+ \\ E_{i+1}^- \end{pmatrix}, \quad (12)$$

T_i being the following matrix:

$$T_i = \frac{1}{t_i} \begin{pmatrix} e^{i\delta_i} & r_i e^{i\delta_i} \\ r_i e^{-i\delta_i} & e^{-i\delta_i} \end{pmatrix}, \quad (13)$$

where $\delta_i = k_p n_i d_i$, n_i is the complex refractive index of the i -th layer, $k_p = 2\pi/\lambda_p$ is the propagation constant in free space, and d_i is the thickness of the layer. r_i and t_i are the amplitude reflection and transmission coefficients at the interface separating the i -th and $(i + 1)$ -th layers, respectively. Assuming that light is incident from only one side of the structure, we set $E_{\text{final}}^- = 0$, thus the electromagnetic field can be expressed as

$$\begin{pmatrix} E_0^+ \\ E_0^- \end{pmatrix} = T_{\text{TOT}} \begin{pmatrix} E_{\text{final}}^+ \\ 0 \end{pmatrix}. \quad (14)$$

The total transfer matrix, T_{TOT} , is given by

$$T_{\text{TOT}} = T_{0\text{H}}(T_{\text{H}}T_{\text{L}})^{(n_{\text{st}}-1)}T_{\text{H}}T_{\text{LD}}[T_{\text{DL}}](T_{\text{L}}T_{\text{H}})^{(n_{\text{st}}-1)}T_{\text{L}}T_{\text{HF}}, \quad (15)$$

where different types of matrices are used in order to satisfy the different boundary conditions: $T_{0\text{H}}$ is the interface matrix at the first boundary of the structure, T_{H} (T_{L}) represents the transfer matrix corresponding to the high (low) index layer, T_{LD} is the matrix of the low index layer at the boundary of the defect and T_{DL} corresponds to the matrix of the defect layer, which is given by

$$T_{\text{DL}} = \frac{1}{t_{\text{DL}}} \begin{pmatrix} e^{i\delta_{\text{D}}} & r_{\text{DL}} e^{i\delta_{\text{D}}} \\ r_{\text{DL}} e^{-i\delta_{\text{D}}} & e^{-i\delta_{\text{D}}} \end{pmatrix}. \quad (16)$$

Here, $\delta_{\text{D}} = k_p n_{\text{D}} L_{\text{D}}$, where n_{D} is the refractive index of the defect, which is given by $n_{\text{D}} = 1 + 1/2\chi_{\text{back}} + 1/2\chi^{(1)}(\omega_{\text{p}}, \Omega_{\text{c}})$, and L_{D} is the length of the defect. Finally, T_{HF} corresponds to the interface of the high index layer at the end boundary of the medium. We want to stress that the wavelength dependence of the refractive index of the defect has been explicitly considered in the numerical calculations. We assume the structure is air surrounded by both sides.

To carry out numerical calculations we design the Bragg structure for operation at a wavelength $\lambda_{\text{pd}} = 9.4115 \mu\text{m}$. For this purpose the length of the defect ($L_{\text{D}} = m\lambda_{\text{pd}}/(2n_{\text{D}}(\Omega_{\text{c}} = 0.5\gamma_2))$, m being an integer) is chosen to obtain resonant operation at this wavelength when the control field is $\Omega_{\text{c}} = 0.5\gamma_2$. In our case, we consider the length of the defect region to be $L_{\text{D}} = 19.97 \mu\text{m}$. In order to get high reflectivity in the Bragg structure, we consider the thickness of the trenches and the teeth given by $d_{\text{L}} = \lambda_{\text{pd}}/(4n_{\text{L}})$ and $d_{\text{H}} = \lambda_{\text{pd}}/(4n_{\text{H}})$, respectively. In particular, we consider that the refractive index of the quantum well regions ($\text{Al}_x\text{Ga}_{1-x}\text{As}$) is $n_{\text{H}} = 3.1977$ whereas that of the trenches (GaAs) is $n_{\text{L}} = 3.157$ at a low temperature around 10 K [24,26]. Thus, the period of the corrugation is 1481 nm. We also consider that the Bragg structure at each side of the defect consists in 100 alternating layers, thus its total length is $74 \mu\text{m}$. With these design parameters, the length of complete structure is $L_{\text{T}} = 168 \mu\text{m}$. In addition, the probe field propagates in the plane of the waveguide while the control field propagates perpendicularly to the probe and illuminates only the defect region for the sake of simplicity. Note that this is not a limiting or essential condition of the structure considered since both the probe and the control fields may co-propagate through it. Both fields are polarized along the growth direction of the quantum wells. The first order susceptibility induced by cross-phase modulation is expressed as Eq. (5) where we assume a typical line center absorption coefficient $\alpha_0 = 10^4 \text{ cm}^{-1}$ [24,26]. Finally, we need to compensate for the residual absorption present near the hole (see Fig. 2a). This task can be accomplished by adding a uniform gain layer to the defect, otherwise the structure could not support the propagating mode. In order to determine the proper gain, we set the gain of this layer to $g_0 = 42 \text{ cm}^{-1}$, which corresponds to the absorption of the system at $\lambda_{\text{pd}} = 9.4115 \mu\text{m}$ and $\Omega_{\text{c}} = 0.5\gamma_2$.

The importance of considering a gain layer can be revealed by inspecting Fig. 3, where the reflectance of the system for different levels of the gain is shown when the control field is set to $\Omega_{\text{c}} = 0.5\gamma_2$. For $g = 0$, i.e. in the absence of gain, there is no coherent interference effect and the structure shows a typical bandgap centered at $\lambda_{\text{pd}} = 9.4115 \mu\text{m}$, the bandwidth being proportional to the index contrast of the corrugated structure (Fig. 3a). When the gain of the layer is set to $g = 0.8g_0$, an incipient mode

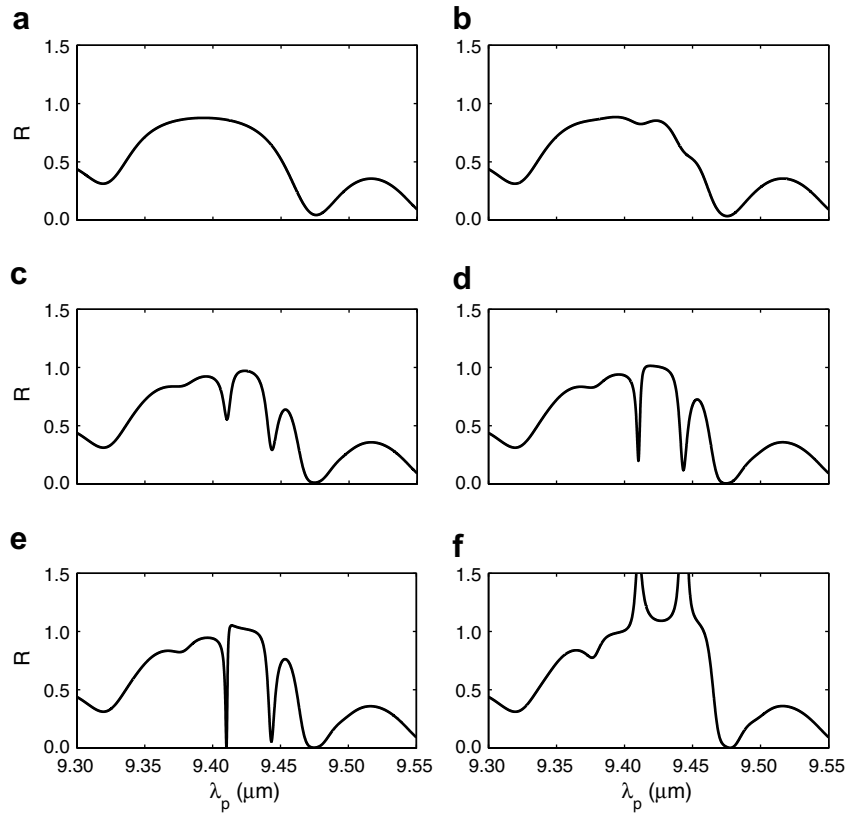


Fig. 3. The reflectivity spectrum of the 1D Bragg structure with a defect, and several values of the gain level. (a) $g = 0$; (b) $g = 0.8g_0$; (c) $g = 0.95g_0$; (d) $g = 0.98g_0$; (e) $g = g_0$; (f) $g = 1.05g_0$. The Rabi frequency of the control field is $\Omega_c = 0.5\gamma_2$.

appears inside the bandgap which corresponds to one of the Fabry–Perot modes of the defect (see Fig. 3b). However, in this case absorption predominates and it explains the weakness of the mode. A further increase of the gain to $g = 0.95g_0$ shows two propagation modes (see Fig. 3c). For $g = 0.98g_0$ the propagation modes become deeper and thinner than in the previous case (see Fig. 3d). In the case that $g = g_0$, which corresponds to the value of the absorption at λ_{pd} and $\Omega_c = 0.5\gamma_2$ (see Fig. 2), one of the modes becomes a fully developed propagation mode with nearly unit transmittance (see Fig. 3e). This behavior is easily understood since absorption experienced by the mode at λ_{pd} is perfectly canceled out by the gain of the layer gain. On the other hand, the absorption on the other mode is greater than gain and the transmittance remains lower than unity. For a gain higher than g_0 the two propagation modes will experience gain (see Fig. 3f). In summary, this figure reveals the essential role of gain in the appearance of a propagating mode. A tuning of the gain of the layer, which is wavelength independent, is required to match the absorption at λ_{pd} , although at other wavelengths gain could exceed absorption of the defect, thus allowing for gain spikes. In subsequent calculations we assume that $g = g_0$.

With the precedent result in mind, Fig. 4 shows the reflectance spectra for different values of the control field. For $\Omega_c = 0$, and $\Omega_c = 0.33\gamma_2$ the gain provided by the gain

layer exceeds the absorption at the wavelength of the two propagation modes and two spikes of gain appear (see Fig. 4a and b). A further increase of the control field to $\Omega_c = 0.49\gamma_2$ produces the appearance of two propagating modes with low reflectance (see Fig. 4c). By setting $\Omega_c = 0.5\gamma_2$ losses are compensated for by gain at λ_{pd} and the propagating mode fully develops (see Fig. 4d). When the Rabi frequency of the control field exceeds the previous value, the spectral width and depth of the propagating mode at λ_{pd} is reduced (see Fig. 4e) and eventually disappears at large Rabi frequencies (see Fig. 4f). These results arise from the increase of the absorption and the enhancement of the refractive index of the defect. In summary, this figure clearly shows that the application of coherent optical processes in the conduction subband transitions of the n-doped QW allows us to control dynamically the optical properties of the defect.

Like in an EIT system, the narrow transmission peak in Fig. 4d is associated with a large optical delay. At the high-Q resonant wavelength of the defect mode, λ_{pd} , light is trapped between the two Bragg reflectors before being transmitted through the device, therefore it experiences a large delay. For any finite medium including gratings, the optical delay can be obtained by evaluating

$$\tau_d = \frac{\partial \arg(T)}{\partial \omega}, \quad (17)$$

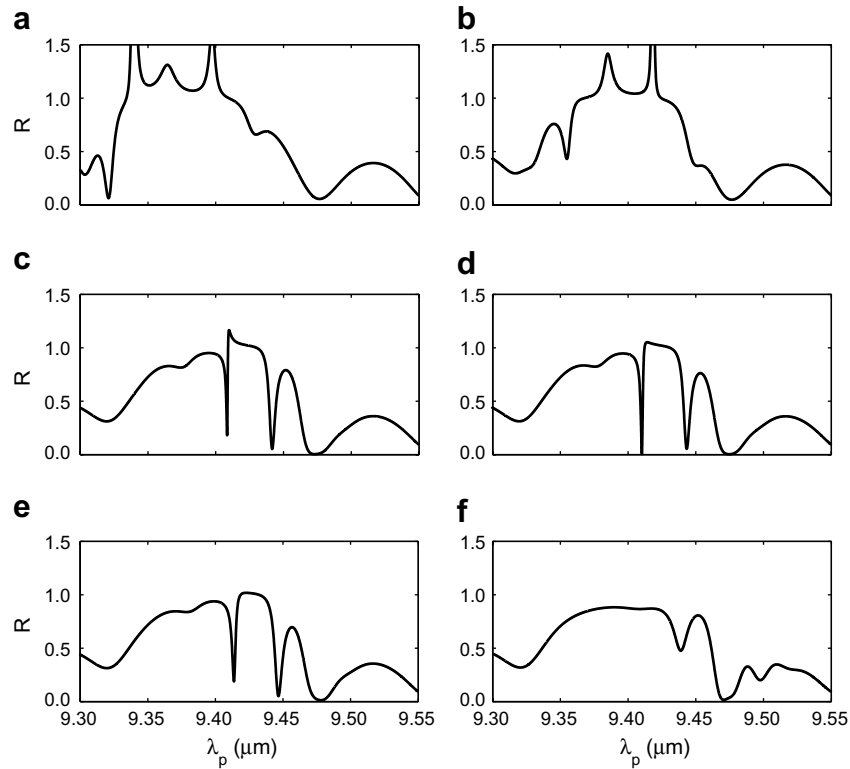


Fig. 4. The reflectivity spectrum of the 1D Bragg structure (a) $\Omega_c = 0$; (b) $\Omega_c = 0.33\gamma_2$; (c) $\Omega_c = 0.49\gamma_2$; (d) $\Omega_c = 0.50\gamma_2$; (e) $\Omega_c = 0.52\gamma_2$; (f) $\Omega_c = 0.65\gamma_2$. The reflectivity contrast at resonance is 0.99. The resonance at $\lambda_{pd} = 9.4115 \mu\text{m}$ allows for the transmission of a small band of light frequencies to be transmitted through the Bragg structure.

where $\arg(T)$ is the argument of the complex transmissivity of the medium. The computed delay spectrum is shown in Fig. 5a. At the bandgap the optical delay increases significantly due to the multiple passes in the cavity, and the peak delay is in the order of ~ 88 ps. Considering that the length of the device in the transmission direction is $\sim 168 \mu\text{m}$, this delay corresponds to an effective group index of ~ 99 , which is on the same order of magnitude as that measured in the slow light regime of photonic crystal waveguides [38]. It must be emphasized that a passive Bragg structure only provides a defect propagation mode with a fixed wavelength. In our case, the presence of the control field intro-

duces a Stark-shift and provides a very sensitive tool for changing the optical path and hence the transmission wavelength of the structure as shown in Fig. 5a. The optical delay τ_d is determined by $\tau_d = T_v - T_m$, T_v/T_m being the time required to propagate through a distance L_T in vacuum/structure. In view of this, $\tau_d < 0 (>0)$ represents delay (advancement) of the pulse.

In Fig. 5b we show a numerical simulation of propagation of a pulse through the 1D Bragg structure which has been carried out using Fourier techniques. We have considered two identical Gaussian pulses centered at λ_{pd} . The width of the pulses is 2 nm. This spectral width corresponds

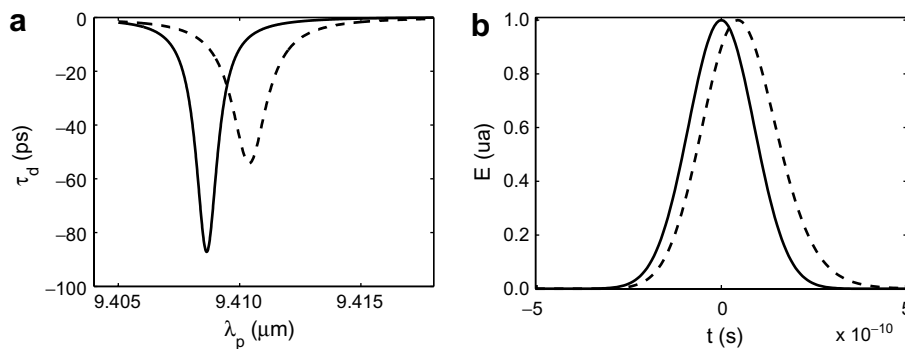


Fig. 5. (a) Optical pulse delay times in the Bragg structure versus the wavelength for two different values of the Rabi frequency of the control field: $\Omega_c = 0.49\gamma_2$ (solid line) and $\Omega_c = 0.51\gamma_2$ (dotted line). (b) Two Gaussian pulses with carrier wavelength $\lambda_{pd} = 9.4115 \mu\text{m}$ one of which propagates through the Bragg structure (dashed line), the other has passed through vacuum (solid line) for the same distance L_T . A delay of 88 ps is obtained.

to the narrow frequency bandwidth of the transmission peak of the propagation mode of the structure. We consider the pulse propagates through the Bragg structure when the control field is set to $\Omega_c = 0.5\gamma_2$ (dashed line) and compare it with the case of vacuum propagation (solid line). In order to estimate the degree of distortion of the transmitted pulse we analyze how the transmitted pulse deviates from the incident Gaussian pulse. To this purpose we have computed the coefficient of asymmetry C_A and kurtosis K of the normalized transmitted pulse $I_T(t) = |E_T(t)|^2/A$, $E_T(t)$ being the transmitted pulse and A is the area under the curve $|E_T(t)|^2$. We remind here that the moment of order k of the distribution $I_T(t)$ can be computed according to

$$\mu_k = \int_{-\infty}^{\infty} (t - \mu_0)^k I_T(t) dt, \quad k = 1, 2, 3 \dots, \quad (18)$$

μ_0 being

$$\mu_0 = \int_{-\infty}^{\infty} t I_T(t) dt. \quad (19)$$

The asymmetry and kurtosis parameters are defined as

$$C_A = \frac{\mu_3}{\sigma^3}, \quad (20)$$

$$K = \frac{\mu_4}{\sigma^4}.$$

It is well known that for a Gaussian distribution these coefficients take the values $C_A = 0$ and $K = 3$, so the deviations from these values of the transmitted pulses will inform us about the distortion produced during propagation. In particular, we obtain values of C_A in the order of 0.28. Concerning the kurtosis parameter K we obtain a value in the order of 3.44 representing a deviation in the order of 13% regarding the non-distorted propagation. In the case of wider in time pulses the level of distortion will be lesser than in the case considered in Fig. 5b.

We are in conditions to analyze to what extent the pulse delay is attributed to the dispersion of the material used for the defect or it arises from structural causes. For this purpose in Fig. 6 we represent the group index derived from the material properties (solid line). In this case the group

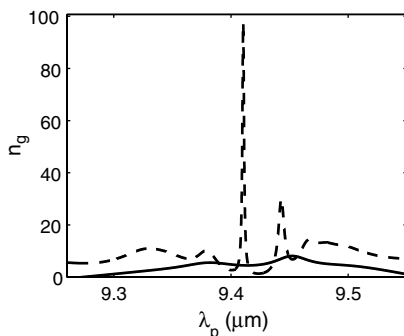


Fig. 6. Group index for the defect itself (solid line) and for the defective Bragg structure (dashed line), for the same value of the control field $\Omega_c = 0.5\gamma_2$.

index depends on the material properties such as electron density, dipolar moments, ... In addition, we represent the group index derived by using Eq. (17) (see dashed line in Fig. 6). It becomes evident that the slow-down factor is enhanced by a factor of 25 due to the Bragg structure.

Finally, it is worth noting that the features of the system make it suitable for an ultrasensitive all-optical switching. The switching operation arises from the development of the propagation mode when the Rabi frequency of the control field is near to the value used for designing the defect ($\Omega_c = 0.5\gamma_2$). The control field shifts the resonance frequency of the Bragg structure through the changes produced in the dispersive properties of the defect. Thus, changes in the value of Ω_c will result in a shift of the reflection peak. Fig. 7 shows the reflectivity versus the wavelength λ_p for different values of the Rabi frequency of the control field. Note that if $\Omega_c = 0.5\gamma_2$, with a corresponding intensity around 10 MW/cm², the sharp transparency appears at $\lambda_{pd} = 9.4115 \mu\text{m}$. In addition, the spectrum has a width in the order of 2 nm (see dashed-dotted line in Fig. 7), which corresponds to a bandwidth of the mode of 7 GHz. This figure reveals that small changes around this bias value for the control field, will produce in turn a shift of the propagating mode, thus the structure will become highly reflective at λ_{pd} . Switching is obtained when the reflection peak is shifted by an amount greater than its width. It is clear from this figure that a change in the Rabi frequency as small as $\delta\Omega_c \approx \gamma_2/100$ would be adequate to produce switching on the reflectance. In order to estimate the sensitivity of such a system, we may consider it as an optical cavity formed by the defect and two Bragg gratings acting as high reflecting mirrors with an effective high reflectance R_{ef} . Thus, the transmissivity of the system can be approximated by

$$T(\omega_p) = \left| \frac{i\Gamma_c}{\omega_p - \omega_m \left(1 - \frac{1}{2} \text{Re}(\chi^{(1)}(\omega_p))\right) + i\left(\Gamma_c + \frac{\omega_{pd}}{2} \text{Im}(\chi^{(1)}(\omega_p)) - g_0\right)} \right|^2, \quad (21)$$

where $\Gamma_c \approx c(1 - R_{ef})/(2L_D R_{ef})$ represents the width due to the coupling to the Bragg gratings, and ω_m is the resonant

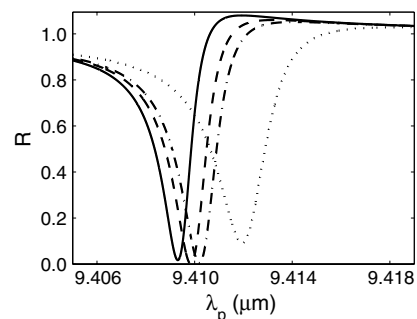


Fig. 7. Reflectance through the Bragg structure at different values of the control field Ω_c . $\Omega_c = 0.495\gamma_2$ (solid line), $\Omega_c = 0.498\gamma_2$ (dashed line), $\Omega_c = 0.5\gamma_2$ (dashed-dotted line), and $\Omega_c = 0.51\gamma_2$ (dotted line).

frequency of the defective cavity in absence of the control field. By inserting the Eq. (8) and (9) into Eq. (21) we arrive to

$$T(\omega_p) \approx \left| \frac{i\Gamma_c}{\omega_p - \omega_m + \frac{c}{v_g}(A_p - s_c) + i\Gamma_c} \right|^2, \quad (22)$$

$v_g = \omega_{pd}N|\mu_{12}|^2/(2\hbar\epsilon_0A^2)$ being the group velocity of the defect itself. Since $\omega_p \approx \omega_m$, Eq. (22) can be further approximated to

$$T(\omega_p) \approx \frac{\left(\frac{c}{v_g}\Gamma_c\right)^2}{(A_p - s_c)^2 + \left(\frac{c}{v_g}\Gamma_c\right)^2}. \quad (23)$$

When the control field is set to the value used to design the active defect ($\Omega_c = \Omega_c^{(0)} = 0.5\gamma_2$), the reflectance of the system exhibits a minimum when $A_p = s_c$ (the propagation mode is fully developed), i.e., the frequency of the propagating mode will be $\omega_{pd} = \frac{c}{v_g} \frac{|\Omega_c^{(0)}|^2}{A_c}$. The shift in this frequency, $\delta\omega$, produced by a change $\delta\Omega_c$ around $\Omega_c^{(0)}$ is $\delta\omega = 2c|\Omega_c^{(0)}|/(v_gA_c)\delta\Omega_c$. To obtain switching, $\delta\omega$ should be greater than $c\Gamma_c/v_g$. Thus we arrive at the following condition

$$\delta\Omega_c \geq \frac{A_c}{2|\Omega_c^{(0)}|} \frac{v_g}{c} \Gamma_c. \quad (24)$$

In the present case, the switching is obtained when $\delta\Omega_c = 0.01\gamma_2$, which is in agreement with numerical simulations. This value $\delta\Omega_c$ obtained corresponds to a change in intensity around 0.2 MW/cm².

4. Conclusions

We have shown the feasibility of tunable optical delay in a one-dimensional Bragg structure formed by a corrugated multi-QW with an active defect inserted at its center. The defect is a double QW which has been modeled as a A - V -type four level system. A change in the refractive index of the defect in the order of 0.4 is achieved via cross-phase modulation. Simulations show that 88 ps optical delay and a group index of 100 can be achieved. The workable spectral window is tens of GHz wide. It is found that the spectral position of the sharp transmission peak appearing in the bandgap can be modified by changing the intensity of the control field. It is shown that delay can be tuned by adjusting the control field with low amplitude variation across the tuning range. The 1D active photonic bandgap may act as an ultrasensitive switch. A simple analytical model is proposed to envisage the underlying physics. Applications are narrowband optical filters with high resolution, delay lines and high-speed optical switches.

Acknowledgement

This work has been supported by Projects No. FIS2004-03267 (MEC, Spain), PR45/05-14183 (UCM/CM, Spain), PR27/05-14019 (UCM/BSCH, Spain), AE5/06-14369

(UCM, Spain), and CCG06-UCM/ESP-1317 (UCM/CM, Spain).

References

- [1] R.W. Boyd, D.J. Gauthier, 'Slow' and 'Fast' Light, in: E. Wolf (Ed.), *Progress in Optics*, vol. 43, Elsevier, Amsterdam, 2002, p. 497, Chapter 6.
- [2] L.V. Hau, S.E. Harris, Z. Dutton, C.H. Behroozi, *Nature* 397 (1999) 594.
- [3] M.M. Kash, V.A. Sautenkov, A.S. Zibrov, L. Hollberg, G.R. Welch, M.D. Lukin, Y. Rostovtsev, E.S. Fry, M.O. Scully, *Phys. Rev. Lett.* 82 (1999) 5229.
- [4] L.J. Wang, A. Kuzmich, A. Dogariu, *Nature* 406 (2000) 277.
- [5] M.S. Bigelow, N.N. Lepeshkin, R.W. Boyd, *Science* 301 (2003) 200.
- [6] J. Marangos, *Nature* 397 (1999) 559.
- [7] D. Dahan, G. Eisenstein, *Opt. Express* 13 (2005) 6234.
- [8] J. Sharping, Y. Okawachi, J. van Howe, C. Xu, A. Willner, Y. Wang, A. Gaeta, *Opt. Express* 13 (2005) 7872.
- [9] Y. Okawachi, M.S. Bigelow, J.E. Sharping, Z. Zhu, A. Schweinsberg, D.J. Gauthier, R.W. Boyd, A.L. Gaeta, *Phys. Rev. Lett.* 94 (2005) 153902.
- [10] J. Sharping, Y. Okawachi, A. Gaeta, *Opt. Express* 13 (2005) 6092.
- [11] K.Y. Song, M.G. Herraes, L. Thevenaz, *Opt. Express* 13 (2005) 82.
- [12] B.S. Ham, P.R. Hemmer, *Phys. Rev. Lett.* 84 (2000) 4080.
- [13] A.V. Turukhin, V.S. Sudarshanam, M.S. Shahriar, J.A. Musser, B.S. Ham, P.R. Hemmer, *Phys. Rev. Lett.* 88 (2002) 023602.
- [14] P.C. Ku, F. Sedgwick, C.J. Chang-Hasnain, P. Palinginis, T. Li, H. Wang, S.W. Chang, S.L. Chuang, *Opt. Lett.* 29 (2004) 2291.
- [15] P. Palinginis, F. Sedgwick, S. Crankshaw, M. Moewe, C. Chang-Hasnain, *Opt. Express* 13 (2005) 9909.
- [16] H. Su, S.L. Chuang, *Opt. Lett.* 31 (2006) 271.
- [17] M. Phillips, H. Wang, *Phys. Rev. Lett.* 89 (2002) 186401.
- [18] M. Phillips, H. Wang, *Opt. Lett.* 28 (2003) 831.
- [19] G.B. Serapiglia, E. Paspalakis, C. Sirtori, K.L. Vodopyanov, C.C. Phillips, *Phys. Rev. Lett.* 84 (2003) 1019.
- [20] L. Silvestri, F. Bassani, G. Czajkowski, B. Davoudi, *Eur. Phys. J. B* 27 (2002) 89.
- [21] A.A. Belyanin, F. Cspasso, V.V. Kocharovsky, VI.V. Kocharovsky, M.O. Scully, *Phys. Rev. A* 63 (2001) 053803.
- [22] P.C. Ku, C.J. Chang-Hasnain, S.L. Chuang, *Electron. Lett.* 38 (2002) 1581.
- [23] S.F. Yelin, P.R. Hemmer, *Phys. Rev. A* 66 (2002) 013803.
- [24] H. Schmidt, K.L. Campman, A.C. Gossard, A. Imamoglu, *Appl. Phys. Lett.* 70 (1997) 3455.
- [25] H. Schmidt, R.J. Ram, *Appl. Phys. Lett.* 76 (2000) 3173.
- [26] J.H. Wu, J.Y. Gao, J.H. Xu, L. Silvestri, M. Artoni, G.C. LaRocca, F. Bassani, *Phys. Rev. Lett.* 95 (2005) 057401.
- [27] B.S. Ham, *Appl. Phys. Lett.* 78 (2001) 3382.
- [28] J. Kim, S.L. Chuang, P.C. Ku, C.J. Chang-Hasnain, *J. Phys.: Condens. Matter* 16 (2004) S3727.
- [29] G. Lenz, B.J. Eggleton, C.K. Madsen, R.E. Slusher, *IEEE J. Quantum Electron.* 37 (2001) 525.
- [30] A. Yariv, Y. Xu, R.K. Lee, A. Scherer, *Opt. Lett.* 24 (1999) 711.
- [31] S. Mookherjea, A. Yariv, *IEEE J. Sel. Top. Quantum Electron.* 8 (2002) 448.
- [32] J. Liu, B. Shi, D. Zhao, X. Wang, *J. Opt. A.: Pure Appl. Opt.* 4 (2002) 636.
- [33] S. Nishikawa, S. Lan, N. Ikeda, Y. Sugimoto, H. Ishikawa, K. Asakawa, *Opt. Lett.* 27 (2004) 2079.
- [34] M.F. Yanik, S. Fan, *Phys. Rev. Lett.* 92 (2004) 083901.
- [35] D.D. Smith, H. Chang, K.A. Fuller, A.T. Rosenberger, R.W. Boyd, *Phys. Rev. A* 69 (2004) 063804.
- [36] M. Scalora, R.J. Flynn, S.B. Reinhardt, R.L. Fork, M.J. Bloemer, M.D. Tocci, C.M. Bowden, H.S. Ledbetter, J.M. Bendickson, J.P. Dowling, R.P. Leavitt, *Phys. Rev. E* 54 (1996) R1078.

- [37] H. Gersen, T.J. Karle, R.J.P. Engelen, W. Bogaerts, J.P. Korterik, N.F. van Hulst, T.F. Krauss, L. Kuipers, *Phys. Rev. Lett.* 94 (2005) 073903.
- [38] Y.A. Vlasov, M. O'Boyle, H.F. Hamann, S.J. McNab, *Nature* 438 (2005) 65.
- [39] S.M. Sadhegi, S.R. Leffler, J. Meyer, *Opt. Commun.* 151 (1998) 173; S.M. Sadhegi, S.R. Leffler, J. Meyer, *Phys. Rev. B* 59 (1999) 15388.
- [40] S. Longhi, *Phys. Rev. E* 72 (2005) 056614.
- [41] S.M. Sadhegi, W. Li, X. Li, W.P. Huang, *Phys. Rev. B* 73 (2006) 035304.
- [42] S.M. Sadhegi, W. Li, *Phys. Rev. B* 72 (2005) 165341.
- [43] M.A. Antón, F. Carreño, Oscar G. Calderón, Sonia Melle, I. Gonzalo, Slow and Fast Light OSA Topical Meeting, Washington DC, 2006.
- [44] Jia-Hua Li, *Phys. Rev. B* 75 (2007) 155329.
- [45] H. Sun, Y. Niu, R. Li, S. Jin, S. Gong, *Opt. Lett.* 32 (2007) 2475.
- [46] S. Minin, M.R. Fisher, S.L. Chuang, *Appl. Phys. Lett.* 84 (2004) 3238.
- [47] P. Ginzburg, M. Orenstein, *Opt. Express* 14 (2006) 12467.
- [48] H. Su, S.L. Chuang, *Opt. Lett.* 31 (2006) 271.
- [49] Q. Xu, J. Shakya, M. Lipson, *Opt. Express* 14 (2006) 6463.
- [50] D. Ahn, S.L. Chuang, *Phys. Rev. B* 34 (1986) R9034.
- [51] A. Yariv, *Quantum Electronics*, John Wiley & Sons, New York, 1987.
- [52] H. Schmidt, A. Imamoglu, *Opt. Commun.* 131 (1996) 333.
- [53] J. Faist, F. Capasso, C. Sirtori, A.L. Hutchinson, K.W. West, L.N. Pfeiffer, *Appl. Phys. Lett.* 71 (1996) 3477.
- [54] D.Y. Oberli, G. Böhm, G. Weimann, J.A. Brun, *Phys. Rev. B* 49 (1994) 5757.
- [55] H. Schmidt, A. Imamoglu, *Opt. Lett.* 21 (1996) 1963.
- [56] S.E. Harris, Y. Yamamoto, *Phys. Rev. A* 64 (1998) 041801.
- [57] M. Yan, E.G. Rickey, Y. Zhu, *Phys. Rev. A* 64 (2001) 041801.
- [58] J. Faist, F. Capasso, C. Sirtori, K.W. West, L.N. Pfeiffer, *Nature* 390 (1997) 589.
- [59] M.D. Frogley, S.R. Leffler, J. Meyer, *Opt. Commun.* 151 (1998) 173.
- [60] Y. Shimizu, N. Shiokawa, N. Yamamoto, M. Kozuma, T. Kuga, L. Deng, E. Hagley, *Phys. Rev. Lett.* 89 (2006) 041112.
- [61] M. Soljačić, E. Lidorikis, J.D. Joannopoulos, *Appl. Phys. Lett.* 86 (2005) 171101.
- [62] P. Bermel, A. Rodríguez, S.G. Jhonson, J.D. Joannopoulos, M. Soljačić, *Phys. Rev. A* 74 (2006) 043818.